Hindawi
Wireless Communications and Mobile Computing
Volume 2018, Article ID 2753025, 15 pages
https://doi.org/10.1155/2018/2753025

Research Article

MC-GiV2V: Multichannel Allocation in mmWave-Based Vehicular Ad Hoc Networks

Wooseong Kim

Department of Computer Engineering, Gachon University, 1342 Seongnam-si, Gyeonggi, Republic of Korea

Correspondence should be addressed to Wooseong Kim; wooseong@gachon.ac.kr

Received 26 February 2018; Revised 2 June 2018; Accepted 10 June 2018; Published 17 July 2018

Academic Editor: Ingrid Moerman

During last several years, mobile communications using mmWave spectrum have been intensively researched for 5G wireless networks. Now the mmWave wireless technologies are evolved into direct device-to-device communications for a single or multihop communication via Giga-bit links. Vehicular ad hoc networks (VANETs) are one of the most attractive areas to apply the direct mmWave communications. In this paper, we propose a Giga-V2V (GiV2V) network, in which vehicles query and deliver high quality video and sensor data of smart and self-driving cars using mmWave communications instead of current dedicated short-range communications (DSRC). In the GiV2V networks, vehicles probably form a grid topology along lanes of a road, which leads to align mmWave beams of the vehicles and cause mutual interference among them. As channel diversity can resolve effectively the interference between mmWave beams, we propose several heuristic algorithms for channel assignment of each beam in the GiV2V networks. We investigate the proposed algorithms using simulation and compare performance with well-known metaheuristic algorithms for this NP-Hard problem.

1. Introduction

5G wireless technology opens a new era of Giga-bit rate data communications using mmWave spectrums for high quality and real-time multimedia data. Many companies and universities built testbeds for measurement study of the mmWave communications and made efforts to demonstrate feasibility of beam forming and tracking developed for mobile communications. The 5G mobile communications are now being standardized in ITU [1], 5GPPP [2], 3GPP [3], and so forth and ready to commercialize. The mmWave communications are also developed for local area communications (e.g., WPAN and WLAN) using 60 GHz unlicensed bands such as IEEE 802.15.3 Task Group 3c (TG3c) [4] and IEEE 802.11ad [5].

Due to severe penetration loss and reflection from short wavelength, mmWave communications are almost feasible only in Line-of-Sight (LoS) environment. When a mmWave link between a sender and receiver is blocked (i.e., non-LoS), relay operation is necessary; in 802.11ad WLAN, the mobile station can access to an access point (AP) via a relay station. Such Device-to-Device (D2D) direct communications using the mmWave spectrum attract attentions to support Giga-bit data rate in proximity services and offloading in cellular networks.

For dissemination of safety messages over roads, V2X communications (e.g., vehicle-to-vehicle, infrastructure, or pedestrian) have been researched and developed intensively during the last decade. At the end, auto companies recently release solutions based on the IEEE 802.11p/WAVE standard which satisfy requirements of safety messages (e.g., low-latency delivery less than 100 *ms*) and support infotainment communications up to 6-27 Mbps using separate service channels. However, a future smart car capable of autonomous driving demands much higher data rate and low latency for vehicle control technology, which relies on large amount of data from near or medium range radars and camera sensors of neighboring vehicles. In particular, higher resolution visual data like Ultra High Definition (UHD) video can enable precise vehicle control; for example, if using 2 M pixel camera instead of 0.3 M in the lane keeping system, curvature recognition accuracy on the front road increases from 30 to 50 *m*, which leads to more safe and fuel efficient driving.

In this paper, Giga-bit vehicle-to-vehicle communication (GiGaV2V or GiV2V) using the mmWave is proposed to support aforementioned high quality multimedia data. Research on the GiV2V has not been conducted popularly and not matured yet to the best of our knowledge. The GiV2V can improve network throughput because of spatial frequency reuse by directional antennas that are typically used to compensate high path loss of the mmWave. However, the spatial division may not occur constructively since vehicles are mostly aligned along lanes of roads and form a grid topology where mmWave beams are also aligned and cause mutual interference. Directivity of the directional antenna increases not only the antenna gain and signal to noise ratio (SNR), but also interferences to other nodes. To mitigate the interference, we propose multichannel- (MC-) GiV2V, a channel diversity scheme in GiV2V networks. Here we introduce several multichannel allocation algorithms with many available channels in the mmWave spectrum; for example, IEEE 802.11ad has 6 channels of each 2 GHz bandwidth.

Our proposed algorithms are distributed, centralized greedy and hybrid algorithms. The distributed algorithm searches a local optimal allocation within an interference region and the greedy algorithm assigns channels based on global information (i.e., SINR of all receive nodes). The hybrid approach is a mixed algorithm of the above two algorithms. Details of algorithms are explained in Section 6. According to simulation results in Section 7, the hybrid approach shows best throughput among them since it probably searches a globally optimal allocation with well-distributed initial conditions. Furthermore, three well-known metaheuristic algorithms are investigated for comparison study with our proposed algorithms.

2. Related Works

Directional antenna was exhaustively exploited for a MAC protocol in multihop ad hoc networks. Most of those researches assume 2.4 or 5 GHz Wi-Fi, but similar challenges also exist in mmWave-based WLANs. Ko et al. [6] first propose a modified 802.11 Distributed Coordination Function (DCF) for directional antennas, which maintains directional channel availability based on the GPS information. Takai et al. [7] use Angle of Arrivals (AOAs) of Request to Send (RTS) and Clear To Send (CTS) instead of GPS information. Choudhury et al. [8] propose a basic directional MAC (DMAC) which includes Directional Network Allocation Vector (DNAV) and listens incoming packets omnidirectionally to trace their Direction of Arrival (DoA). Kolar et al. [9] introduce a greed queuing to solve a Head of Line (HoL) problem with the DNAV table of beam directions. Ramanathan et al. [10] suggest different backoff algorithms for different events such as busy channel and missing CTS or ACK and also tight power control scheme. In order to solve a hidden terminal problem in the DMAC, Circular Directional RTS (CDR) [11], CRCM [12], and DtD-MAC [13] conduct sequential RTS and CTS transmissions to all directions, which deals with deafness and directional hidden terminals from unheard nodes or asymmetric antenna gain. But the circular transmissions suffer from control overhead and excessive delay according to number of sectors. Gossain et al. [14] propose simultaneous circular RTS/CTS to reduce the delay with Diametrically Opposite Direction (DOD) which removes duplicate transmissions of RTSs and CTSs in the overlapped area. Furthermore, Deafness Avoidance and Collision Avoidance (DMAC-DACA) [15] and DMAC with Deafness Avoidance (DMAC/DA) [16] reduce circular transmission overhead by DNAV reservation and beam direction information, with which nodes can determine spatial diversity and schedule pending transmitters. Singh et al. [17] propose a Memory-guided DMAC (MDMAC), as a fully distributed MAC protocol, which enables approximate TDM scheduling for wireless meshes using the memory about transmission success or fail.

Recently, mmWave communications emerge as one of the key 5G technologies. Its feasibility has been explored by many universities and companies. Rappaport et al. [18] perform measurement campaign in New York City on the 28 GHz, 38 GHz, and 73 GHz bands [19, 20] and establish a channel model of the mmWave communications. The mmWave links are considered not only for access links of mobile devices, but also for backhaul links that can constitute wireless mesh networks [21, 22]. 3GPP [3] completes standards of a new radio (i.e., mmWave communications) and now moves into device-to-device communications for the mmWave which can be applied to legacy proximity services in cellular networks.

The mmWave for WLANs has already been explored for home and mobile appliances at indoor environment. Also, several standards using 60 GHz unlicensed bands were released such as IEEE 802.15.3 Task Group 3c (TG3c) [4] and IEEE 802.11ad [5], which specify physical and MAC protocols (Carrier Sensing Multiple Access/Collision Avoidance (CSMA/CA), Time Division Multiple Access (TDMA), etc.). Also, those WPAN/WLAN standards define relay operation that can be utilized for multihop ad hoc networks. For instance, an access point (AP) arranges service periods (SPs) for Directional Multi-Giga-bit (DMG) mobile stations (STAs), when the AP receives a request of Relay DMG STA (RDS) search from a STA for NLOS environment. During the SPs, a source and destination STA exchange the packets with candidate RDSs nearby. Then, the source STA asks several RDSs with good channel (i.e., high SNR) to report channel condition to both source and destination STAs. Finally, the source STA selects a best RDS that has highest SNR in both links.

In [23], demanded rate-based coordination of the directional or omnidirectional transmissions is proposed with allocation of time slots for spatial and time reuse of frequency in mmWave WLANs. Sing et al. [24] propose a multihop MAC protocol for indoor mmWave environment where diffraction and blockage highly occur due to fixed or moving obstacles (e.g., people and furniture). They develop a diffraction model to estimate link connectivity and decide multihop relays. From simulation, it is proved that proposed approach improves network throughput with low overhead rather than an AP-based single hop communication. Reference [25] describes tactical scenarios using mmWave links for a secure channel in military ad hoc networks and relay operation in NLOS environment. In [26], a CSMA/CA-like MAC protocol

for directional mmWave is proposed. Chen et al. [27] propose a spatial reuse strategy with directional antennas in IEEE 802.11 ad networks. Son et al. [28] propose a Frame based Directive MAC protocol (FDMAC) which is a centralized scheduling algorithm for the Pico-Net Controller (PNC) based on greedy coloring providing multiple concurrent transmissions. Thornburg et al. [29] analyze throughput of ad hoc networks using mmWave communications. Authors establish a 2D-PPP model of nodes and obstacles deployment and evaluate performance of one- or two-way communications in terms of SINR and coverage with simulation. In [30], Park et al. propose a Multiband Directional Neighbor Discovery (MDND) for self-organization of ad hoc networks, which utilizes dual radios with different bands and antenna types, a 2.4 GHz band with an omnidirectional antenna and 60 GHz band with a directional antenna. Reference [31] proposes a stochastic model of vehicular communications at highway for mmWave communications, where mmWave-based road side units are deployed for infrastructure to vehicle communications with high data rate rather than vehicle-to-vehicle communications. Blockage probability according to vehicle density and speed is shown from the model. In [32], authors show design and implementation of a long-range and broadband aerial communication system with directional antennas (ACDA), which enables unmanned aerial vehicle (UAV) to extend communication range, increase throughput, and reduce interference. In the testbed, the ACDA achieves 48 Mbps throughput at a distance of 300 m and 2 Mbps at 5000 m, promising long-distance Wi-Fi aerial communication. Reference [33] proposes joint optimization to select relay and link to get around obstacle and reduce delivery latency in 60 GHz mmWave networks and develops a less complex algorithm by decomposing the problem into subproblems. In [34], research results on propagation characteristics for V2V channels, particularly shadowing effects induced by obstructing vehicles between transmitter (Tx) and receiver (Rx), are introduced. In [35], measurement campaign is conducted in the mmWave band for the 12 most common railway materials; influence of typical objects to the mmWave propagation channel is analyzed for railway scenarios with various configurations. Reference [36] proposes an IEEE 802.11ad-based radar for long-range radar (LRR) applications at the 60 GHz unlicensed band, which enables a joint waveform for automotive radar and mmWave vehicle-to-vehicle communications reusing hardware.

3. GiV2V Network Architecture

Figure 1 depicts an architecture of GiV2V networks, in which vehicles deployed at an intersection form mmWave beams toward neighbor vehicles to exchange safety and infotainment data. Also, they can share own storage or processing power to maintain floating data and process those data. For instance, video clips captured in the intersection area are held and analyzed by vehicles or road side units (RSUs) for object or event detection [37]. In order to query and deliver the floating data in this vehicular cloud, the Information Centric Networking (ICN) mechanism can be used [37–39].

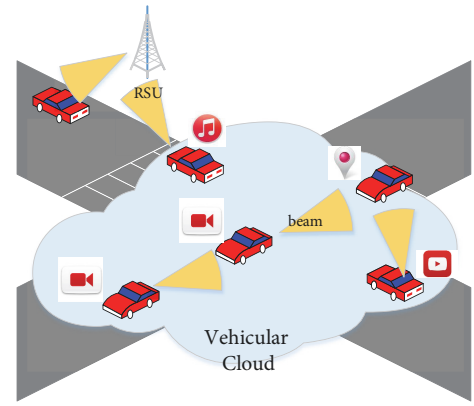

Figure 1: GiV2V network architecture.

Due to road structure, neighbor vehicles are located on limited positions, which are mostly front, back, and side directions as shown in Figure 2. First, a simple convoy model of Figure 2(a) is a typical traffic pattern at roads and appropriate to create a vehicle flow (i.e., vehicle train) for autonomous driving of smart cars. In this model, transmission direction is also limited, forward or backward, which can cause considerable interference among vehicles without transmission power control. However, de- and acceleration of vehicle speed lead to varying distance between vehicles, so the power control probably makes vehicle connectivity unstable. Second, a vehicle searches vehicles in next lanes with side beams to couple partitioned networks along the lanes as shown in Figure 2(b). This scenario can cause more interference than the convoy model due to small lane width. The beam directions are more various according to road shapes (e.g., curve and intersection), road width (e.g., multilane highway), and vehicle speed. Accordingly, vehicles can be located on front side or rear side in next lanes as shown in Figure 2(c). Such diagonal beams diverse beam directions like a random topology that has lower interference than a grid topology of Figures 2(a) and 2(b). However, the grid topology has advantages in connection establishment with small efforts to sweep beam directions compared to the random topology. As a consequence, most of the beams in GiV2V communications belong to scenarios in Figure 2, and considerable interference can exist due to limited beam directions.

4. Directional Antenna

4.1. Directivity Model. In this paper, a beamforming model is expressed by a sectorized directional antenna following ITU-R reference [40] that covers 400 to 70 GHz spectrum as below. The radiation intensity at azimuthal $F(\phi)$ and elevation plane $F(\theta)$ is modelled by two different radiation intensity functions: rectangular and exponential sectoral radiation.

Directivity of omnidirectional and sectoral antennas is

$$D = \frac{U_M}{U_0}, \tag{1}$$

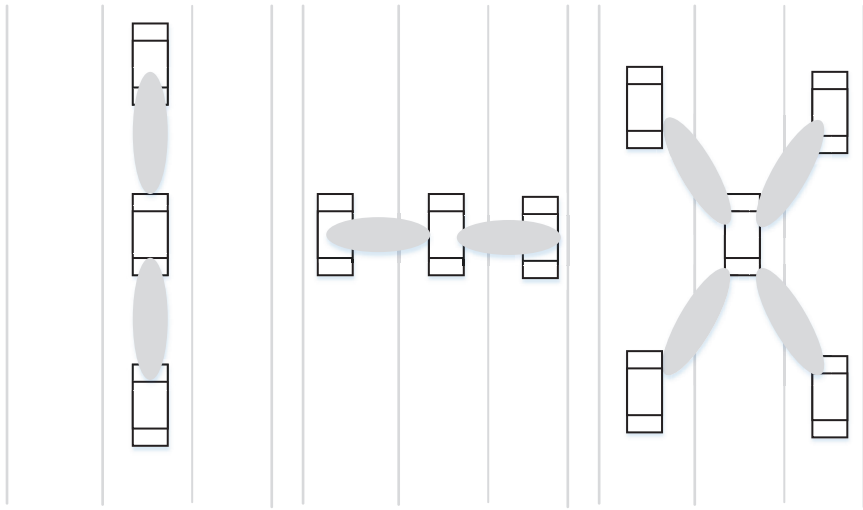

(a) Front-rear beam (b) Side beam (c) Front-rear side beam

Figure 2: GiV2V topology and beam pattern at road.

where D is directivity (i.e., gain) and U_0 is radiation intensity of an isotropic source.

$$P_t = \int_0^{2\pi} \int_0^{\pi} F(\theta) F(\phi) \sin(\theta) \, d\theta d\phi, \tag{2}$$

then the omnidirectional power is $U_0 = 1/4\pi P_t$.

Here those two different radiation intensity functions in the azimuthal plane can be considered while the elevation plane is assumed to be an exponential function. In rectangular sectoral radiation, the azimuthal power intensity is derived as

$$F(\phi) = \begin{cases} 0 & \text{if } \dfrac{\phi_s}{2} - |\phi| \geq 0 \\ 1 & \text{if } \dfrac{\phi_s}{2} - |\phi| < 0 \end{cases} \tag{3}$$

And elevation power is

$$F(\theta) = e^{-a\theta^2}, \quad a = -\ln(0.5) \frac{4}{\theta_{bw}}, \tag{4}$$

where θ_{bw} is beamwidth.

Accordingly, the omnidirectional intensity is calculated approximately as

$$U_0 = \frac{\phi_s \theta_{bw}}{4\pi} \sqrt{\frac{\pi}{2.773}} e^{-\theta^2/11.09} \tag{5}$$

The directivity D_r of the rectangular radiation model is

$$D_r = \frac{38750}{\phi_s \theta_{bw}} e^{\theta_{bw}^2/36400}, \tag{6}$$

when U_M is 1.

In the exponential function for sectoral radiation, the azimuthal function $F(\phi)$ is replaced by the following exponential function:

$$F(\phi) = e^{b\phi^2}, \quad b = \ln(0.5) \frac{4}{\phi_s^2} \tag{7}$$

Here the gain D_e of the exponential radiation model is

$$D_e = \frac{36400}{\phi_s \theta_{bw}} e^{\theta_{bw}^2/36400} \tag{8}$$

Side lobes are smaller than the main lobes with the front-to-back ratio (FBR) (i.e., ratio of front-side lobes) denoted by γ ($0 < \gamma \leq 1$, 1 for omnidirection). Accordingly, the gains of a main lobe and side lobes are $G_m = (1 - \gamma) D(\theta_{bw})$ and γG_m, respectively. Table 1 shows gains of main and side lobes with varying γ values.

For our experiment that appeared in Section 7, 30, 60, and 90 degrees of beam width are used; the directivity antenna gains are 16.8, 8.4, and 5.6 dBi, respectively. While the widths of those beams are in a linear scale, gains increase exponentially as shown in Figure 3.

4.2. Coverage in GiV2V Networks. Figure 4 shows an example of communication range in GiV2V networks. The coverage is varying according to beam directions of neighbor vehicles in contrast to a coverage using omnidirectional antenna. In the figure, 10 vehicles exit near the transmitter V_t but only 4 vehicles, from V_{r1} to V_{r4}, have connection to the transmitter. Supposing that the transmitter vehicle, V_t, forms a beam shadowed among 4 sectors (i.e., 90 degrees), the receiver vehicle V_{r1} located on the transmission sector is reachable even with its different beam direction in the d_2 coverage. However, other V_{r2} and V_{r3} that are not on the first quarter sector but within the d_2 must create beams toward the transmitter V_t for connections. In the d_3 coverage, only the V_{r4} has a connection to the V_t since both the transmitter and receiver have to beam to each other.

Table 2 describes beamforming gain and corresponding reachable radio ranges. When antenna gain from bore sight of a main lobe is denoted as G and gain from other directions is g as a side lobe, vehicles in d_3 should have beamforming to each other and in d_2, one of a sender and receiver has to make a beam to a peer node at least.

Table 1: Gain of main and side lobes.

	Directivity (Gain)	γ=0.2	γ=0.5	γ=0.7
90	5.613824327	1.122765	2.806912	3.929677
60	8.42073649	1.684147	4.210368	5.894516
45	11.22764865	2.24553	5.613824	7.859354
30	16.84147298	3.368295	8.420736	11.78903
15	33.68294596	6.736589	16.84147	23.57806
10	50.52441894	10.10488	25.26221	35.36709

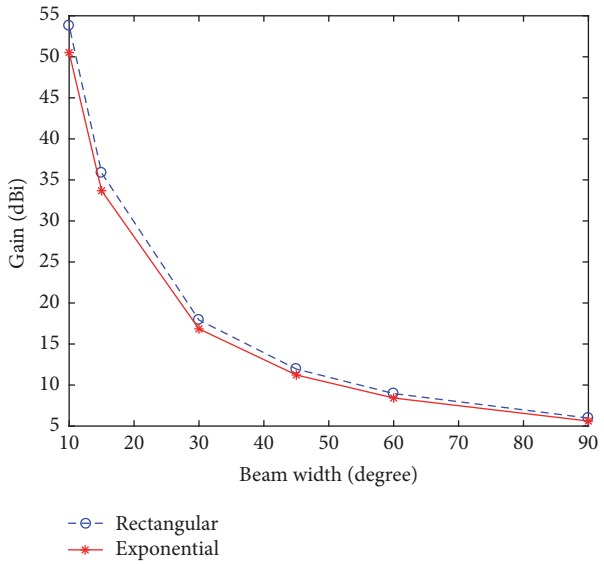

Figure 3: Directivity (gain) of rectangular and exponential radiation models.

5. mmWave Channel Propagation Model

The mmWave pathloss model at 60 GHz was established for LoS environment based on measurement study [41].

$$L_d\,(dB) = A + 20\log_{10}\left(f_{MHz}\right) + 10\alpha\log_{10}\left(d\right), \quad (9)$$

where the A is 32.5 dB and no shadow factor. d is a distance between a transmitter and receiver (km) and α is a pathloss exponent of LoS (e.g., 2).

In outdoor GiV2V communication, additional attenuation from vapour water (L_{vap}), oxygen (L_{O_2}), and rain (L_R) is considered as below. Total pathloss can be $PL(d) = L_{(f,d)} + L_a$.

$$L_a\,(dB) = d\left(L_{vap} + L_{O_2} + L_R\right). \quad (10)$$

Those atmosphere parameters (dB/km) for further loss are assumed constant for relatively short communication period in this study [42, 43]. From simplicity of the constant L_a during the short communication period, the path loss is only determined by the distance, d, at a given operational frequency, f (e.g., 60 GHz).

$$P_r = P_t - PL\,(d) - NF + G_R + G_T - IL - CB, \quad (11)$$

where P_r and P_t are transmission and receive power and NF and N_{th} are noise floor and thermal noise. Maximum antenna gain, G_T, G_R of a transmitter T and receiver R is assumed to be the same (i.e., same antenna array). IL is implementation loss like from cables CB.

Table 2: Beam direction and radio range.

Gain	Range
G_t G_r	d3
G_t g_r	d2
g_t G_r	d2
g_t g_r	d1

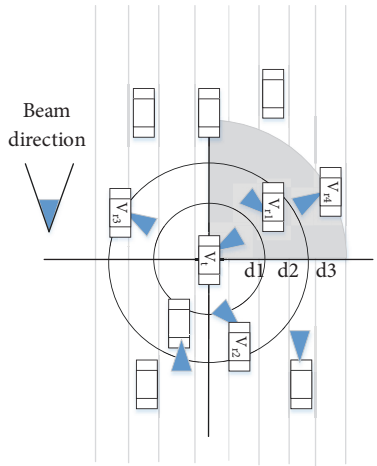

Figure 4: Varying coverages in GiV2V networks.

In the LoS environment, the radio range can be derived by the following outage probability with a required SNR of a target Modulation Coding Scheme (MCS).

$$P\left(P_r \geq T\right) = P\left(PL\left(d\right) \leq P_t + G_R + G_T - T - G_n\right), \quad (12)$$

where $PL(d)$ is pathloss of distance d, T is sensitivity for the required MCS level, and $G_n = NF + IL + CB$. For instance, minimum T is -78 or -68 dBm for control signals and data with lowest MCS, $\pi/2$-BPSK, respectively.

In the above equation, maximum coverage d can be calculated by $PL^{-1}(P_t + G_R + G_T - T - G_n)$. Accordingly, the effective range is decided by only antenna gain of transmission and reception (i.e., beamforming factor) as shown in Table 2 while other parameters are assumed to be constant; in this study,

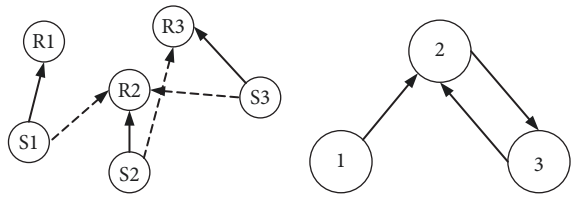

(a) Network topology (b) Interference relation

Figure 5: GiV2V topology and interference.

no transmission power control is achieved between vehicles. From (12), maximum range, d, can be expressed as follows.

$$d = \left(\frac{P_t G_R G_T}{T G_n} \right)^{1/\alpha} \tag{13}$$

Consequently, the coverage is exponentially increasing with beamforming gain according to the (13).

6. Multichannel Beamforming for GiV2V Networks

The GiV2V enables multiple vehicles to create mmWave links to near vehicles with directional beams for concurrent Giga-bit communications. Those beams can be aligned or diversified according to network topologies and interference also occurs by the beam patterns.

Figure 5(a) illustrates an example of interfering 3 pairs of communication vehicles with directional beams, where each vertex indicates a vehicle node, sender *Sn*, and receiver *Rn*, and receive interference is different to each pair because of adjacent beam directions; *R*2 receives interference from both transmitters *S*1 and *S*3 denoted as dashed lines, while *R*3 has interference only from *S*2 and there is no interference for *R*1. The interference among nodes can be expressed by a directed graph as in Figure 5(b) in which each vertex indicates a pair of communication nodes, i.e., a link or beam.

In the interference graph of the GiV2V networks, multiple channels can be assigned to the vertices for collision and interference avoidance. For example, only 2 channels can remove the mutual interference completely in Figure 5(b): CH1 for vertexes 1 and 3 and CH2 for vertex 2. This channel assignment for each communication pair is a coloring problem of the interference graph, which is a combinatorial problem known as a NP-Hard. Accordingly, we propose several algorithms that can be realized in centralized or distributed manners and compare their performance through simulation.

6.1. System Model. We build a system model to design and analyze our algorithms. We define variables according to the directed interference graph in Figure 5(b). Each communication link is denoted as a vertex and directional interference as an edge; there are i vertices and ij directional edges. Symbols of the our system model are described in Table 3.

Table 3: System model parameters.

Symbol	Description
N	A set of communication links
C	A set of available channels
G	Directional antenna gain
P	Power of transmission
B	Bandwidth
r_i	Data rate at link i
L	Path loss
d	Distance between vehicles

The channel assignment for each link $i \in N$ can be expressed by x_i^c. If the link i is tuned to the channel c,

$$x_i^c = \begin{cases} 1, & i \text{ on } c \\ 0, & \text{otherwise.} \end{cases} \tag{14}$$

Data rate of a communication link, i, on a channel c, r_i^c, can be calculated approximately by Shannon and Friis transmission equation as follows:

$$r_i^c = B_c \log_2 \left(1 + \frac{P_i G_i \Lambda L_i x_i^c}{\sigma^2 + \sum_{j:j \in H_i} P_k G_j \Lambda L_j x_j^c} \right), \tag{15}$$

where $\Lambda = (\lambda/4\pi)^2$ and $L_i = d_i^\alpha$. The α is an exponent for free-space pathloss and d is distance of a communication link or an edge of Figure 5(b). Other parameters are denoted in Table 3. Afterwards the distance term is only used for the interference edge rather than the other. H_i is a hyperarc that consists of set of incoming edges at the vertex i in the interference graph. For an example of Figure 5(b), $H_1 = \{\}$, $H_2 = \{1, 3\}$, and $H_3 = \{2\}$. System bandwidth B_c can be 2.1 GHz for each channel according to IEEE 802.11ad.

In this study, our objective is maximizing sum of utility of each communication link.

$$\max \sum_i U\left(r_i^c\right) \tag{16}$$

The utility function U is defined as follows.

$$U\left(r_i^c\right) = \gamma + \kappa \sum_{i \in N} \sum_{c \in C} x_i^c r_i^c, \tag{17}$$

where γ is minimum data rate for a pair of communication nodes on a channel c and κ is a small value like 1e-3 for max-min fairness among links [43].

6.2. Random Channel Assignment. Each link is the same as a vertex. To clarify, each link (a vertex in the interference graph) chooses a channel randomly in a distributed manner, which is mostly simple and powerful compared to complicated channel assignment algorithms. In addition, vehicle nodes can use position information (i.e., GPS) for random seeds to diversify channel selection within an interference region.

6.3. Distributed Channel Assignment. As the same distributed approach, neighboring nodes can exchange channel selection information to avoid collisions rather than the random selection, which enables nodes to select a minimum used channel within interference region. In this section, we introduce a simple Distributed Channel Assignment (DCA) algorithm.

The achievable rate of each link is varying by the channel assignment in the system model, which is intractable. Accordingly, the objective is redefined as a local general assignment problem to minimize maximum aggregated gain within interference region from (15). For the simplicity, fixed transmission power and constant parameters are omitted. This local solution from the redefined problem does not guarantee to find a global optimum, but it is valuable for notable throughput and easily realized in the distributed architecture.

$$\text{minimize} \quad \max_{c} \sum_{i \in H} w_i x_i^c \tag{18}$$

$$\text{subject to} \quad w_i = G_i d_i^{-\alpha} \tag{19}$$

$$\sum_{c \in C} x_i^c = 1, \quad i \in N \tag{20}$$

$$x_i^c \in \{0, 1\}, \quad i \in N, \ c \in C, \tag{21}$$

where the interference weight w_i is decided by distance to an interferer and beam direction. The hyperarch H is one of interference regions in a whole network. Equation (18) can be reformulated into an equivalent epigraph form and solved by Lagrangian relaxation as follows.

$$\text{minimize} \quad \text{t} \tag{22}$$

$$\text{subject to} \quad \sum_{i \in H} w_i x_i^c \le t \tag{23}$$

$$\text{Eq. (20)} - (21) \tag{24}$$

Partial Lagrangian can be derived for relaxation by dualizing first constraint (23),

$$\begin{aligned} L(t, x, \boldsymbol{\lambda}) &= t + \sum_{c \in C} \lambda_c \left(\sum_{i \in H} w_i x_i^c - t \right) \\ &= t \left(1 - \sum_{c \in C} \lambda_c \right) + \sum_{i \in H} \sum_{c \in C} \lambda_c w_i x_i^c, \end{aligned} \tag{25}$$

where λ is nonnegative Lagrange multiplier for the first inequality constraint (23). Accordingly, we can have a dual function $g(\lambda) = L(t, x, \boldsymbol{\lambda})$ by minimizing above partial Lagrangian with regard of x and t, where the dual function can have $-\infty$ by t if $\sum_{c \in C} \lambda_c \neq 1$. Therefore, we can redefine the dual function with constraint for λ.

$$\text{maximize} \quad g(\boldsymbol{\lambda}) \tag{26}$$

$$\text{subject to} \quad \sum_{c \in C} \lambda_c = 1 \tag{27}$$

$$\lambda_c \ge 0 \tag{28}$$

```
1: procedure VehicleChannelSelectFunc
2:     Initialization: λ_c(t) for all c, and estimate w_i
3:     loop:
4:     Select c ⟵ arg min_c λ_c w_i according to Eq.(29)
5:     Broadcast the selected channel c, x_i^c
6:     Update λ_c(t + 1) according to Eq.(30).
7:     if λ_c(t) = λ_c(t + 1) then
8:         stop;
9:     Broadcast λ_c(t)
10:    goto loop.
```

Algorithm 1: Distributed channel selection algorithm.

In this dual problem, the analytical solution for the combinatorial problem can be derived in a closed form expression. For optimal x^*,

$$x_i^{c*} = \begin{cases} 1, & \text{c} = \text{c}* \\ 0, & \text{otherwise}, \end{cases} \tag{29}$$

where the optimal channel ($c^* = \arg\min_c \lambda_c w_i$) from (25) can be easily found, which is one minimizing sum of weight within the interference range by choosing minimum prices, $\boldsymbol{\lambda}$. Accordingly, the derivation of the $\mathbf{x}$ only takes $O(N)$ linear time.

The dual function is convex although it is not differentiable. Therefore optimal λ value in (26) can be acquired using a subgradient method. A following projected subgradient method updates the λ value by given channel allocation, $\mathbf{x}$, with which the algorithm newly assigns channels to nodes to converge into an optimum.

$$\lambda_c(t + 1) = \lambda_c(t) + \alpha_t \sum_{i \in H} w_i x_i^{c*}, \tag{30}$$

where t indicates an algorithm iteration and α_t is a tth step size ($\alpha_t > 0$).

Above the closed form solution can be realized in distributed manner as shown in Algorithm 1.

6.4. Interference-Aware Channel Assignment. In contrast to the local solution introduced in Algorithm 1, we propose a greedy SINR-based Channel Assignment (SCA) algorithm in a centralized architecture, where vehicles report chosen channels to a controller and then the controller calculates optimal allocation for the objective. As shown in (17) and (18), our objective is minimizing maximum aggregated interference. Thus, the controller chooses a link with maximum aggregated interference and assigns a separate channel first as a greedy manner. Algorithm 2 explains a procedure of the algorithm to assign a channel to each link based on degree of interference. First, the algorithm selects a pair of vehicles that suffer from highest interference and assigns a channel that brings maximum throughput enhancement in overall networks. The algorithm continues until no more link can have gain after changing own channel.

1: **procedure** ControllerGreedyScheduleFunc
2: Initialization: $c = 1$ and $x_i^1 = 1$
3: Receive $\sum_{j \in H_i} w_j$ from i
4: MAX = $\sum_i \sum_{j \in H_i} w_j$
5: *loop*:
6: $i \longleftarrow \arg\max_i \sum_{j \in H_i} w_j$
7: $c^* \longleftarrow \arg\min_c \sum_{j \in H_i} w_j x_j^c$
8: **if** MAX > $\sum_i \sum_{j \in H_i} w_i$) **then**
9: Update $c = c^*$, $x_e^c = 0$ and $x_e^{c^*} = 1$
10: MAX = $\sum_i \sum_{j \in H_i} w_j$)
11: **goto** *loop*.
12: **else**
13: **stop**;

Algorithm 2: Greedy channel selection algorithm.

6.5. Hybrid Channel Assignment. Previously proposed SCA algorithm assumes no initial channel distribution; all vehicles have the same channel (e.g., channel 1) at the beginning. However, it is not realistic and able to lead the algorithm to reach local maxima. Therefore, we propose an initialized SCA (InitSCA) algorithm as a hybrid approach that utilizes the DCA and SCA in sequence; the DCA allows vehicles to find a local optimum and then a controller of the SCA adjusts channel allocation based on SINR of each pair of communication vehicles to enhance total network throughput.

7. Experiments

In this section, we evaluate channel allocation algorithms introduced in Section 6 using simulations. In GiV2V networks, vehicles communicate with one-hop neighbors regardless of a final destination at a certain time. Previous studies about a directional MAC show that a HoL problem can be solved by a neighbor location table and scheduling order [9, 44]. From this, we assume that a vehicle has a communication peer nearby and establish a beam toward the peer node.

We consider an exemplary scenario at highway that has a simple vehicle traffic pattern with varying vehicle densities and uses wireless local area (WLAN) networking for V2V communications. This GiV2V network topology at the highway follows 2D-PPP that is shown similar with a PPP model along multiple lanes in terms of average throughput [45]. For simulation parameters, the highway space is 20 x 400 m and vehicle density is varying from 3 to 11e-3. Transmission power of each node is configured as 20 dBm in the WLAN and the channel model is applied as shown in Section 5.

Average distance $\mathbb{E}(D)$ between vehicles can be derived by the PPP model as follows. 2D-Poisson distribution with density λ is

$$\mathbb{P}\left(\Phi\left(A\right) = n\right) = e^{-\lambda|A|} \frac{\left(\lambda\left|A\right|\right)^n}{n!} \tag{31}$$

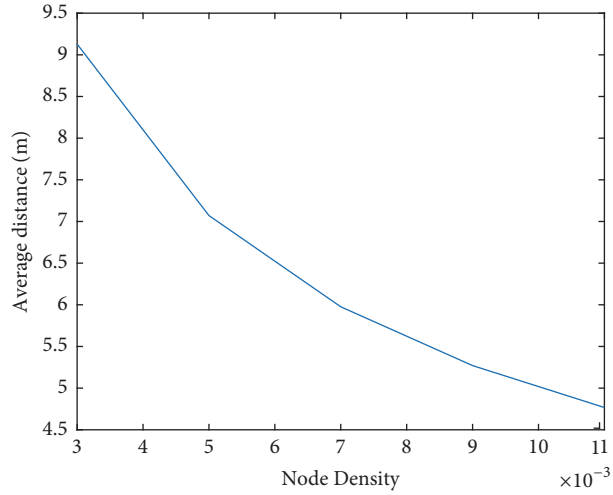

Figure 6: Average distance by vehicle density.

Then the CCDF of the distance of the nearest point of the process is the same as probability of empty set in circle area of a radius, r, $\mathbb{P}(\Phi(\pi r^2) = 0)$.

$$\mathbb{P}\left(D > r\right) = e^{-\lambda \pi r^2} \tag{32}$$

Hence average distance can be calculated as

$$\mathbb{E}\left(D\right) = \int_0^\infty f\left(r\right) r dr = \frac{1}{2\sqrt{\lambda}}, \tag{33}$$

where the PDF $f(r)$ of the nearest point is given from the CCDF as below.

$$f\left(r\right) = 2\pi r \lambda e^{-\lambda \pi r^2} \tag{34}$$

Figure 6 shows the average distance with varying vehicle density. Density 3e-3 shows average 9 m distance to the nearest node while density 11e-3 shows less than 5 m. According to this average distance, SNR of a link to the nearest node is plotted in Figure 7 based on the channel model discussed in Section 5. The SNR increases as the vehicle density grows because path loss reduces by decreasing link distance to a neighbor node. Furthermore, the SNR is varying by directivity gain as shown in Figure 3 (also refer to Table 1). The SNR increases as the number of sectors decreases; in 4 sectors, the SNR is around 6 dB while it is much higher in 6 and 12 sectors, about 10 and 27 dB, respectively, in Figure 7. Also, beam alignment affects the SNR; in particular, a narrower beam causes more difference in SNR. For instance, there is only a 4 dB gap between Gg and gg in 4 sectors, but 15 dB in 12 sectors (beam alignments Gg and gg described at Table 2). In this study, the Gg or gg case is only for interference since we assume that all communication pairs tune to each other. Here we can conclude that the GiV2V can suffer from higher interference by the aligned network topologies, in which a node can receive GG interference in addition to the Gg and gg.

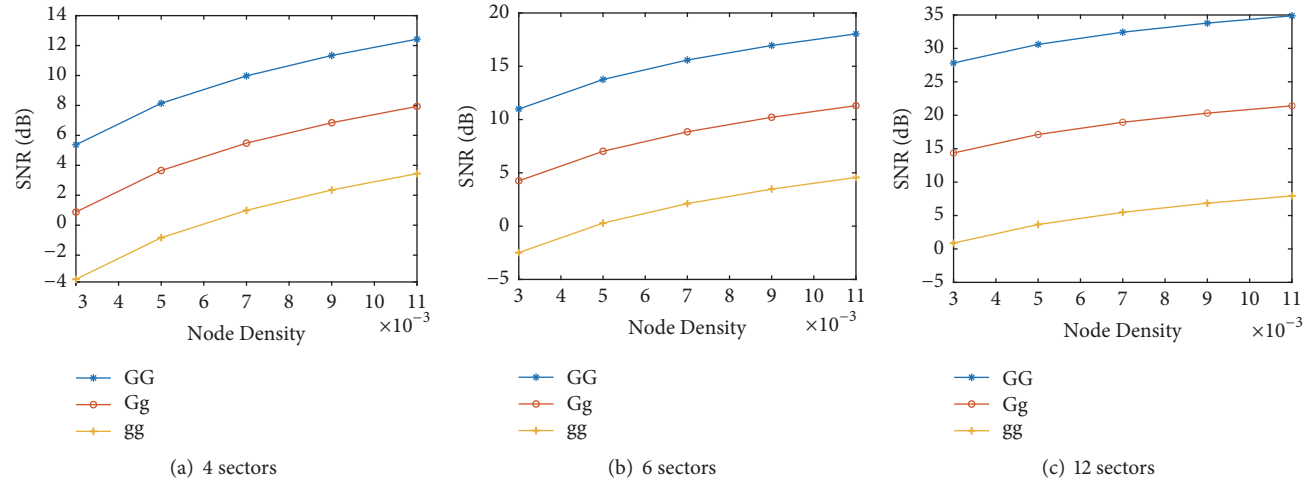

(a) 4 sectors (b) 6 sectors (c) 12 sectors

Figure 7: Average SNR of the shortest GiV2V link.

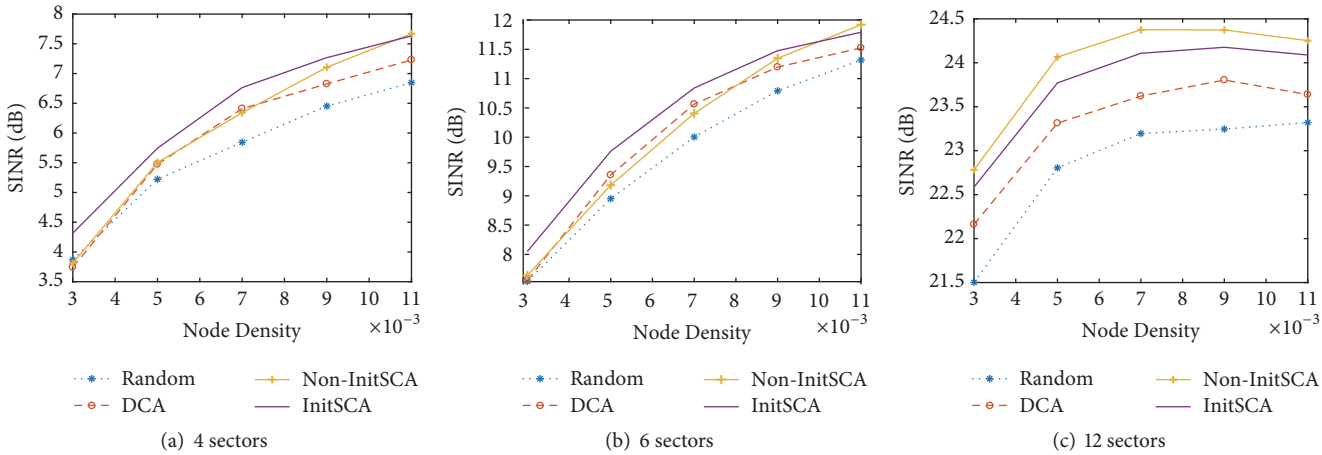

(a) 4 sectors (b) 6 sectors (c) 12 sectors

Figure 8: Average SINR with 3 channels.

7.1. Comparison of Proposed Algorithms. We compare our 4 channel assignment algorithms in a PPP highway model with varying density of vehicles. To obtain average throughput, total 200 runs with random topologies are conducted. Each vehicle chooses nearest another randomly as a receiver or relay and transmits data. Transmission power is 20 dBm, and topology change due to vehicle mobility is not considered.

Figure 8 shows average SINR of transmission links at different node densities when applying each algorithm with 3 channels. Performance shows a similar pattern regardless of number of sectors. The random allocation achieves the lowest throughput while the InitSCA mostly outperforms others. Noninitialized SCA (later called just SCA) and DCA approaches are comparable. In particular, the SCA shows better throughput in 12 sectors than the InitSCA because of increasing interference from narrow beams.

Here we observe that the node density and antenna directivity affect SINR with different degree of interference. For instance, node density 3e-3 has about 6 dB for SNR in Figure 7(a) and 4 dB as SINR in Figure 8(a) with interference in case of the random assignment, while node density 11e-3 has almost 12 dB SNR but only 7 dB for SINR. In other words, the higher node density 11e-3 suffers more interference, 2 versus 5 dB reduction. For the directivity, Figure 7(c) shows more or less 30 dB SNR in node density 3e-3 and SINR of the same density is 20 dB in case of the random algorithm in Figure 8(c). Thus, almost 10 dB reduction occurs due to the interference in 12 sectors, which is much higher than the case of 4 sectors, 2 dB reduction because nodes can cause stronger interference and interference coverage expansion with high directivity. The interference becomes severe as the density increases; in 12 sectors, node density 11e-3 shows that 35 dB SNR is degraded to only 23 dB SINR in case of the random algorithm.

Figure 9 shows experiment results with 6 channels (e.g., IEEE 802.11ad channels), which allows more degree of freedom for interference avoidance. Compared to 3 channel results, low density allows comparable throughput among all algorithms because of orthogonality in space and channel divisions. However, as density grows, gaps among algorithms

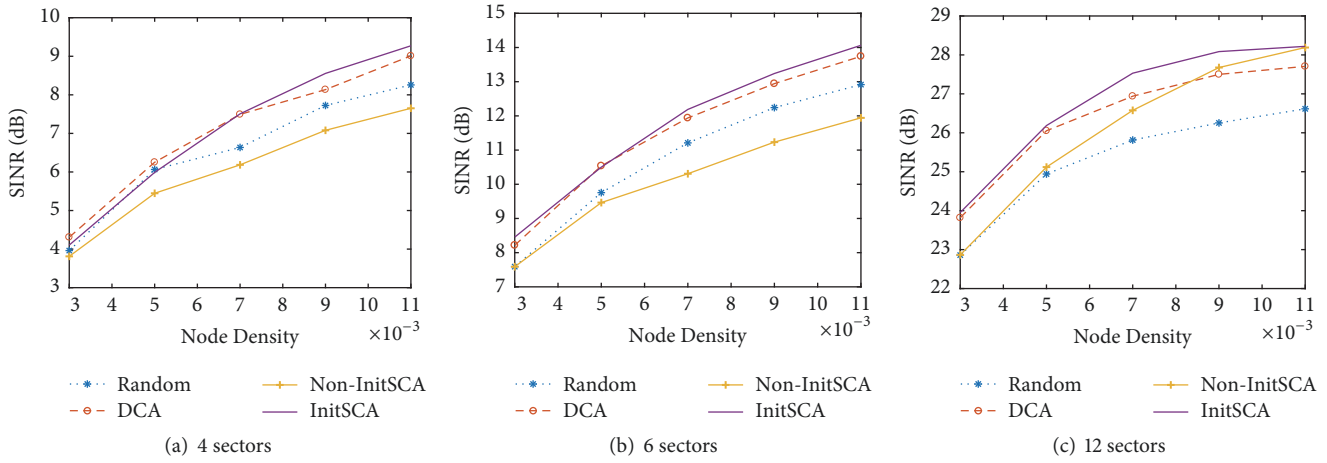

Figure 9: Average SINR with 6 channels.

increase; the SCA achieves lower throughput than others including the random algorithm. From this, the SCA algorithm is assumed to stop at a local maximum while the random or DCA mechanism searches a solution closer to a global optimum. However, the SCA shows bit better performance in 12 sectors than the random and DCA distributed algorithms since the high interference avoidance may reduce overall average SINR.

Figures 10 and 11 show standard deviation and 0 dB probability (i.e., a level of lowest MCS) of SINR of results in Figure 9. Standard deviation indicates difference of SINR among transmission links. Thus, the max-min-like SCA reduces the difference effectively because it assigns a channel first to a link that has worst SINR compared to others. The InitSCA shows lower deviation than the DCA by adjusting channel assignment for some links with low SINR. In low density, the deviation is affected mostly by length of each link while the deviation is determined by interference in high density. Figures 10(a) and 10(b) show that the deviation of the SCA and InitSCA is consistent or decreasing while the deviation of others increases; increasing interference from node density is effectively managed in case of the SCA and InitSCA compared to others. Furthermore, the probability that is less than 0-dB shows clearly max-min fairness achievement of the SCA in Figures 11(a) and 11(b). Similar with the deviation, the SCA has the lowest probability of 0-dB SINR among algorithms and shows robustness with increasing density. In 12 sectors, the 0-dB probability of the SCA is almost zero because of high spatial diversity; other algorithms' probabilities are also quite lower than ones of 6 sectors. Note that the probability decreases as the density grows because of path loss reduction. As a result, multihop relays can be effective rather than direct communications in dense GiV2V networks.

Figure 12 depicts throughput with reduced transmission power, 10 dBm instead of 20 dBm. A total of 6 channels are assigned to nodes. Compared to results in Figure 9(a), SINR decreases, for an example of the 4 sectors, from 9 to 2 dB in high density due to Tx power reduction as shown in Figure 12(a). In low density, SINR shows less than 0 dB, i.e., -4 dB. Also, SINR difference among algorithms decreases, which implies that throughput difference from varying channel diversity gain becomes reduced as interference effect reduces. However, the throughput gap increases again as the interference increases due to high beam directivity in Figure 12(c). Transmission power control can reduce interference but together with receive signal strength that mainly affects the throughput rather than the interference that can be avoidable by spatial or channel diversity.

7.2. Comparison of Global Optimization Algorithms. According to experiment results in Section 7.1, the InitSCA is the most effective algorithm among proposed algorithms across all densities and sectors. In this section, we compare the InitSCA performance with three well-known metaheuristic algorithms for seeking a global optimum, which are popularly used for large scale optimization and NP-Hard problems. For this comparison, we apply the same parameters used in the simulation of Section 7.1. Actual global optimum can be found by exhaustive search algorithms like brand and bound, but its average value (e.g., from 200 runs) requires much computation time due to the complexity of experiment scenario.

Here we introduce briefly those three algorithms: Simulated Annealing (SA) [46], Generic Algorithm (GA) [47], and Particle Swarm Optimization (PSO) [48]. First, the SA follows a physical annealing analogy, in which heated particles in a liquid state are cooled down slowly to reach thermal equilibrium. In the algorithm, the particles are converged into lowest energy level by probability that moves to a new state, which decreases to zero along the cooling temperature. Here final energy level is determined by cooling speed; slow cooling leads to acquire a global optimum but delay might not be negligible for real-time systems. In our system, we limit number of iterations as 1e4. Second, the GA follows a process of natural DNA evolution, which is based on DNA operations such as mutation, crossover, and selection.

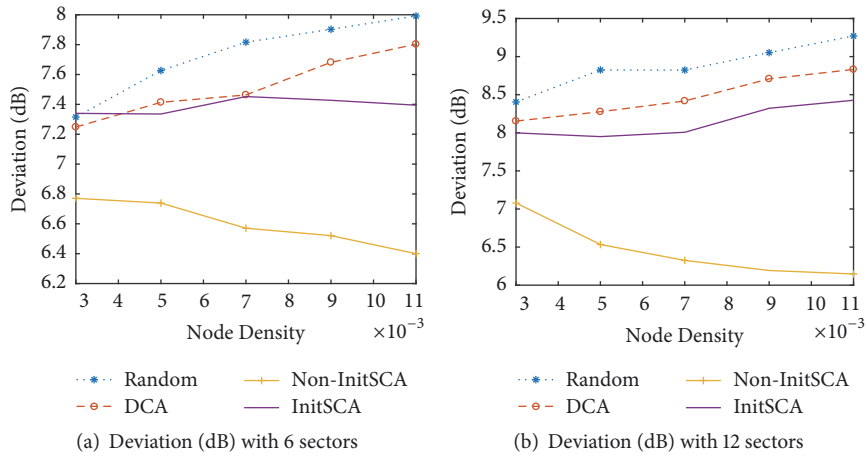

(a) Deviation (dB) with 6 sectors (b) Deviation (dB) with 12 sectors

Figure 10: Standard deviation with 6 channels.

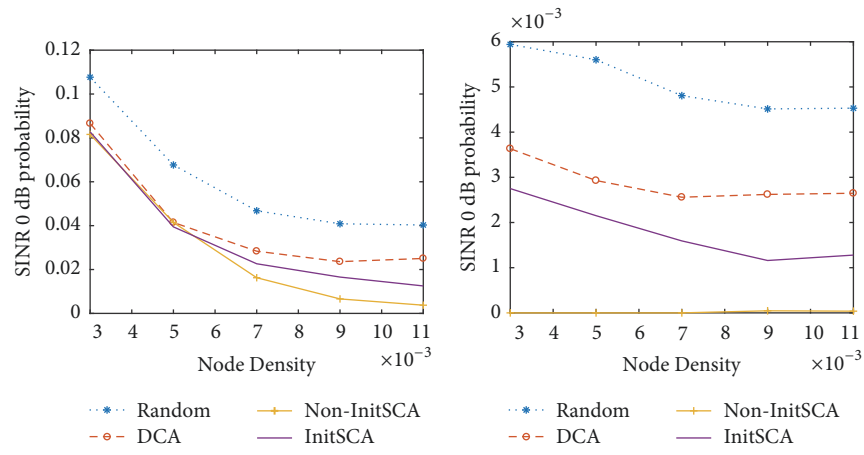

(a) SINR 0 dB probability with 6 sectors (b) SINR 0 dB probability with 12 sectors

Figure 11: Zero SINR probability with 6 channels.

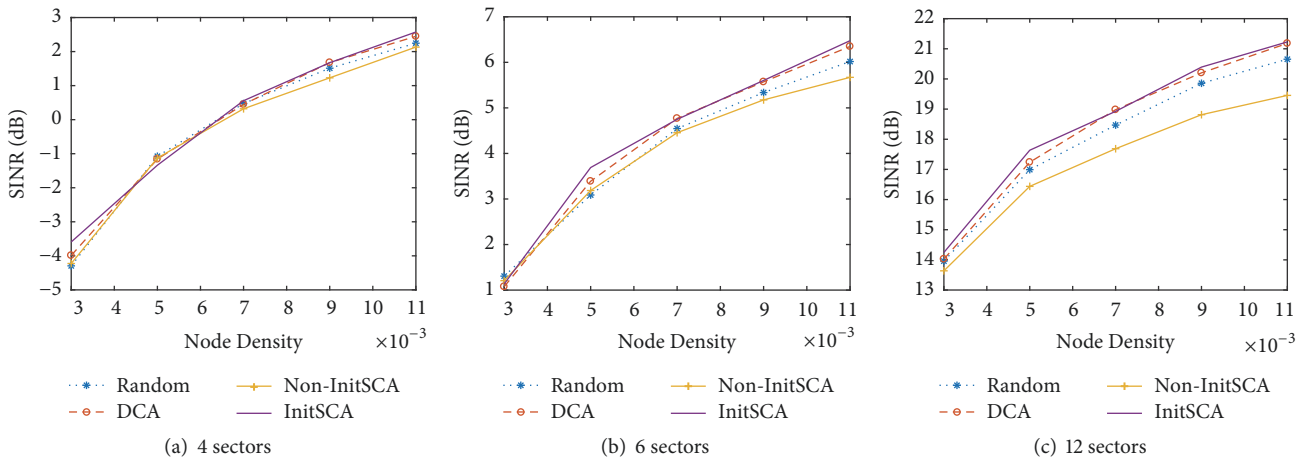

(a) 4 sectors (b) 6 sectors (c) 12 sectors

Figure 12: Average SINR with Tx power, 10 dBm.

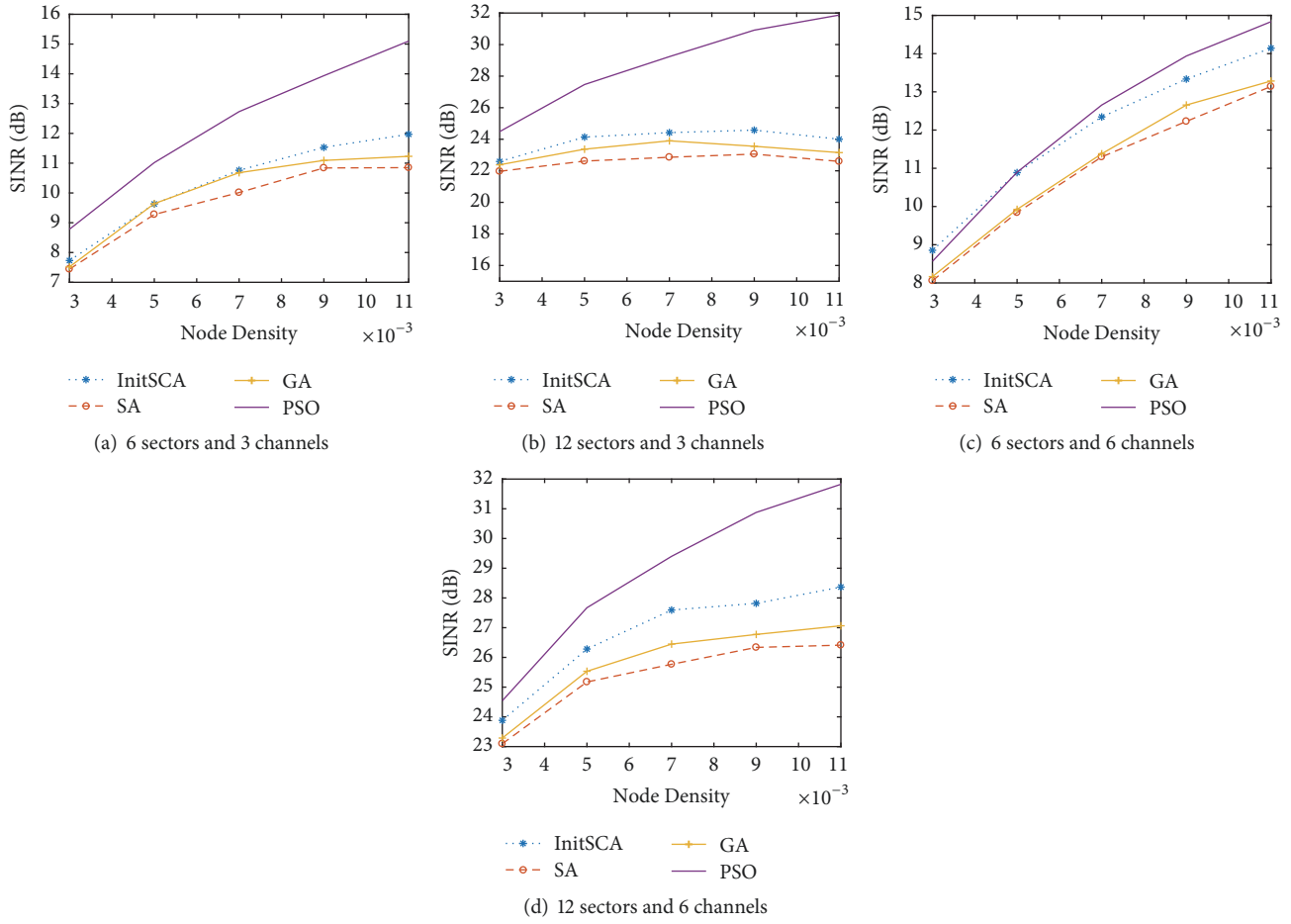

Figure 13: Average SINR of global optimization algorithms.

Candidate solutions are evolved and selected by such bio-inspired operations until finding a global optimum. Third, PSO generates similarly swarm of particles as candidate random solutions, in which particles search for better solutions in the search space according to swarm's best known position and find optima by updating generations. Compared to the GA, PSO is easy to implement with a few parameters to adjust for simple formulae.

Figure 13 shows average SINR of algorithms with varying channels and sectors. In all cases, PSO outperforms other algorithms, especially for 12 sectors. InitSCA is comparable with the GA or SA in case of 3 channels regardless of sectors. With 6 channels, the InitSCA shows slightly better throughput, about 1 dB than the GA and SA. Consequently, the GA and SA probably do not reach a global optimum although they are good solutions. Optimization of SA and GA such as cooling speed and crossover strategy in order to find the optimum is left for our future works.

Metaheuristic algorithms require conventionally considerable search time which is inappropriate for real-time applications like wireless communications. In the GiV2V networks, channels should be reassigned according to topology change; the GiV2V can have a new topology in a couple of seconds considering vehicle speed. Time complexity of our algorithm is shown as $O(n)$ in Section 6.5, but other metaheuristic algorithms have different complexity with a population size (refer to [49] for each complexity). Table 4 and Figure 14 show average elapsed time for the global algorithms at each node density. The initialized SCA takes only several ten milliseconds for all density cases, but SA and GA consume about 5 to 35 seconds; time increases drastically according to the node density. Due to this long delay, those two algorithms are hard to apply to the GiV2V networks. PSO delay, less than 2 seconds at highest density, seems competitive considering its performance shown in our simulation.

8. Conclusion

In this study, we propose a new VANET architecture, GiV2V, using mmWave spectrum and investigate its performance with simulation. Beamforming for mmWave links can increase receive signal quality and overcome high propagation loss of the mmWave. However, it can also cause higher interference in beam-aligned ad hoc networks, especially in high node density. In this study, we propose a simple distributed algorithm and centralized greedy algorithm based

Table 4: Elapsed time of global algorithms.

	3e-3	5e-3	7e-3	9e-3	11e-3
InitSCA	0.006994	0.014559	0.024938	0.041612	0.067441
SA	4.525196	8.652447	14.37165	22.30713	32.49279
GA	1.811456	4.840629	13.46396	24.10401	37.83527
PSO	0.385824	0.625597	0.92461	1.237252	1.665746

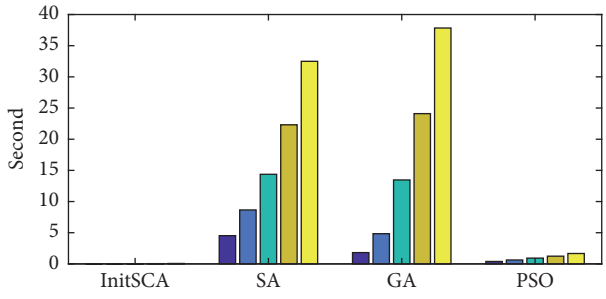

Figure 14: Average computation time of algorithms with increasing density (5 λ from 3e-3 to 11e-3).

on SINR. Although the centralized algorithm outperforms distributed one, the distributed algorithm is still competitive at high degree of freedom from many channels and less complicated to implement. The centralized greedy algorithm shows comparable throughput with several metaheuristic algorithms while its complexity is lower and appropriate for real-time GiV2V systems. We will experiment further to evaluate the proposed algorithms under vehicle mobility simulation and look for optimum values using branch and bound algorithm to compare as future works.

Data Availability

The data used to support the findings of this study are available from the corresponding author upon request.

Conflicts of Interest

The author declares that there are no conflicts of interest.

Acknowledgments

This research was supported by Basic Science Research Program through the National Research Foundation of Korea (NRF) funded by the Ministry of Science and ICT (no. NRF-2017R1C1B1006607).

References

[1] "ITU," https://www.itu.int/.

[2] "5GPPP," https://5g-ppp.eu/.

[3] "3GPP," http://www.3gpp.org/.

[4] "IEEE, "IEEE 802.15.3 Working Group, Part 15.3: Wireless Medium Access Control (MAC) and Physical Layer (PHY) Specifications for High Rate Wireless Personal Area Networks (WPANs), IEEE Unapproved Draft Std P802.15.3c/D10," bibtex:ieee80215c.

[5] *Part11: Wireless LAN Medium Acess Control (MAC) and Physical Layer (PHY) Specifications C Amendment 5: Enhancements for Very High Throughput in the 60 GHz Band*, 2010, IEEE P802.11ad/D1.0.

[6] Y.-B. Ko, V. Shankarkumar, and N. H. Vaidya, "Medium access control protocols using directional antennas in ad hoc networks," in *Proceedings of the INFOCOM 2000. Nineteenth Annual Joint Conference of the IEEE Computer and Communications Societies*, 2000.

[7] M. Takai, J. Martin, A. Ren, and R. Bagrodia, "Directional virtual carrier sensing for directional antennas in mobile ad hoc networks," in *Proceedings of the MOBIHOC 2002: PROCEEDINGS OF The Third ACM International Symposium on Mobile Ad Hoc Networking and Computing*, pp. 183–193, Switzerland, June 2002.

[8] R. R. Choudhury, X. Yang, R. Ramanathan, and N. H. Vaidya, "Using directional antennas for medium access control in ad hoc networks," in *Proceedings of The Eight Annual International Conference on Mobile Computing and Networking*, pp. 59–70, USA, September 2002.

[9] V. Kolar, S. Tilak, and N. Abu-Ghazaleh, "Avoiding head of line blocking in directional antenna [MAC protocol]," in *Proceedings of the 29th Annual IEEE International Conference on Local Computer Networks. LCN 2004*, pp. 385–392, Tampa, FL, USA.

[10] R. Ramanathan, J. Redi, C. Santivanez, D. Wiggins, and S. Polit, "Ad hoc networking with directional antennas: A complete system solution," *IEEE Journal on Selected Areas in Communications*, vol. 23, no. 3, pp. 496–506, 2005.

[11] T. Korakis, G. Jakllari, and L. Tassiulas, "CDR-MAC: A protocol for full exploitation of directional antennas in ad hoc wireless networks," *IEEE Transactions on Mobile Computing*, vol. 7, no. 2, pp. 145–155, 2008.

[12] G. Jakllari, I. Broustis, T. Korakis, S. V. Krishnamurthy, and L. Tassiulas, "Handling asymmetry in gain in directional antenna equipped ad hoc networks," in *Proceedings of the IEEE 16th International Symposium on Personal, Indoor and Mobile Radio Communications (PIMRC '05)*, vol. 2, pp. 1284–1288, IEEE, Berlin, Germany, September 2005.

[13] E. Shihab, L. Cai, and J. Pan, "A distributed asynchronous directional-to-directional MAC protocol for wireless ad hoc networks," *IEEE Transactions on Vehicular Technology*, vol. 58, no. 9, pp. 5124–5134, 2009.

[14] H. Gossain, C. Cordeiro, and D. P. Agrawal, "MDA: An efficient directional MAC scheme for wireless ad hoc networks," in *Proceedings of the GLOBECOM'05: IEEE Global Telecommunications Conference, 2005*, pp. 3633–3637, USA, December 2005.

[15] Y. Li and A. M. Safwat, "DMAC-DACA: Enabling efficient medium access for wireless ad hoc networks with directional

antennas," in *Proceedings of the 2006 1st International Symposium on Wireless Pervasive Computing*, pp. 1–5, Thailand, January 2006.

[16] M. Takata, M. Bandai, and T. Watanabe, "A MAC protocol with directional antennas for deafness avoidance in ad hoc networks," in *Proceedings of the 50th Annual IEEE Global Telecommunications Conference, GLOBECOM 2007*, pp. 620–625, USA, November 2007.

[17] S. Singh, R. Mudumbai, and U. Madhow, "Distributed coordination with deaf neighbors: efficient medium access for 60 GHz mesh networks," in *Proceedings of the IEEE Conference on Computer Communications (INFOCOM '10)*, pp. 1–9, March 2010.

[18] T. Rappaport, S. Sun, R. Mayzus et al., "Millimeter wave mobile communications for 5G cellular: it will work!," *IEEE Access*, vol. 1, pp. 335–349, 2013.

[19] S. Sun, G. R. Maccartney, M. K. Samimi, S. Nie, and T. S. Rappaport, "Millimeter wave multi-beam antenna combining for 5G cellular link improvement in New York City," in *Proceedings of the 1st IEEE International Conference on Communications (ICC '14)*, pp. 5468–5473, IEEE, Sydney, Australia, June 2014.

[20] G. R. Maccartney Jr. and T. S. Rappaport, "73 GHz millimeter wave propagation measurements for outdoor urban mobile and backhaul communications in New York City," in *Proceedings of the 1st IEEE International Conference on Communications (ICC '14)*, pp. 4862–4867, Sydney, Australia, June 2014.

[21] P. Wang, Y. Li, L. Song, and B. Vucetic, "Multi-gigabit millimeter wave wireless communications for 5G: from fixed access to cellular networks," *IEEE Communications Magazine*, vol. 53, no. 1, pp. 168–178, 2015.

[22] C. Dehos, J. González, A. de Domenico, D. Ktéenas, and L. Dussopt, "Millimeter-wave access and backhauling: the solution to the exponential data traffic increase in 5G mobile communications systems?" *IEEE Communications Magazine*, vol. 52, no. 9, pp. 88–95, 2014.

[23] X. An and R. Hekmat, "Directional MAC protocol for millimeter wave based wireless personal area networks," in *Proceedings of the IEEE 67th Vehicular Technology Conference-Spring (VTC '08)*, pp. 1636–1640, May 2008.

[24] S. Singh, F. Ziliotto, U. Madhow, E. M. Belding, and M. Rodwell, "Blockage and directivity in 60 GHz wireless personal area networks: from cross-layer model to multihop MAC design," *IEEE Journal on Selected Areas in Communications*, vol. 27, no. 8, pp. 1400–1413, 2009.

[25] S. L. Cotton, W. G. Scanlon, and B. K. Madahar, "Millimeter-wave soldier-to-soldier communications for covert battlefield operations," *IEEE Communications Magazine*, vol. 47, no. 10, pp. 72–81, 2009.

[26] M. X. Gong, R. Stacey, D. Akhmetov, and S. Mao, "A directional CSMA/CA protocol for mmWave wireless PANs," in *Proceedings of the IEEE Wireless Communications and Networking Conference 2010, WCNC 2010*, Australia, April 2010.

[27] Q. Chen, X. Peng, J. Yang, and F. Chin, "Spatial reuse strategy in mmWave WPANs with directional antennas," in *Proceedings of the IEEE Global Communications Conference (GLOBECOM '12)*, pp. 5392–5397, Anaheim, Calif, USA, December 2012.

[28] I. K. Son, S. Mao, M. X. Gong, and Y. Li, "On frame-based scheduling for directional mmWave WPANs," in *Proceedings of the IEEE Conference on Computer Communications (INFOCOM '12)*, pp. 2149–2157, March 2012.

[29] A. Thornburg, T. Bai, and J. Heath, "Performance analysis of outdoor mmWave ad hoc networks," *IEEE Transactions on Signal Processing*, vol. 64, no. 15, pp. 4065–4079, 2016.

[30] H. Park, Y. Kim, T. Song, and S. Pack, "Multiband directional neighbor discovery in self-organized mmWave Ad Hoc networks," *IEEE Transactions on Vehicular Technology*, vol. 64, no. 3, pp. 1143–1155, 2015.

[31] A. Tassi, M. Egan, R. J. Piechocki, and A. Nix, "Modeling and Design of Millimeter-Wave Networks for Highway Vehicular Communication," *IEEE Transactions on Vehicular Technology*, vol. 66, no. 12, pp. 10676–10691, 2017.

[32] J. Chen, J. Xie, Y. Gu et al., "Long-Range and Broadband Aerial Communication Using Directional Antennas (ACDA): Design and Implementation," *IEEE Transactions on Vehicular Technology*, vol. 66, no. 12, pp. 10793–10805, 2017.

[33] Z. He, S. Mao, S. Kompella, and A. Swami, "On Link Scheduling in Dual-Hop 60-GHz mmWave Networks," *IEEE Transactions on Vehicular Technology*, vol. 66, no. 12, pp. 11180–11192, 2017.

[34] Q. Wang, D. W. Matolak, and B. Ai, "Shadowing Characterization for 5 GHz Vehicle-to-Vehicle Channels," *IEEE Transactions on Vehicular Technology*, 2017.

[35] D. He, B. Ai, K. Guan et al., "Influence of Typical Railway Objects in mmWave Propagation Channel," *IEEE Transactions on Vehicular Technology*, 2017.

[36] P. Kumari, J. Choi, N. Gonzalez Prelcic, and R. W. Heath, "IEEE 802.11ad-based Radar: An Approach to Joint Vehicular Communication-Radar System," *IEEE Transactions on Vehicular Technology*, 2017.

[37] M. Gerla, E.-K. Lee, G. Pau, and U. Lee, "Internet of vehicles: from intelligent grid to autonomous cars and vehicular clouds," in *Proceedings of the IEEE World Forum on Internet of Things (WF-IoT '14)*, pp. 241–246, March 2014.

[38] E. Lee, E.-K. Lee, M. Gerla, and S. Y. Oh, "Vehicular cloud networking: architecture and design principles," *IEEE Communications Magazine*, vol. 52, no. 2, pp. 148–155, 2014.

[39] W. Kim, "Beyond LTE-advance for information centric networking," *Computer Standards & Interfaces*, vol. 49, pp. 59–66, 2017.

[40] "F.1336: Reference radiation patterns of omnidirectional, sectoral and other antennas for the fixed and mobile service for use in sharing studies in the frequency range from 400 mhz to about 70 ghz".

[41] A. Maltsev, R. Maslennikov, A. Sevastyanov, A. Khoryaev, and A. Lomayev, "Experimental investigations of 60 GHz WLAN systems in office environment," *IEEE Journal on Selected Areas in Communications*, vol. 27, no. 8, pp. 1488–1499, 2009.

[42] E. Zola, A. J. Kassler, and W. Kim, "Joint user association and energy aware routing for green small cell mmWave backhaul networks," in *Proceedings of the 2017 IEEE Wireless Communications and Networking Conference, WCNC 2017*, USA, March 2017.

[43] W. Kim, "Dual Connectivity in Heterogeneous Small Cell Networks with mmWave Backhauls," *Mobile Information Systems*, vol. 2016, 2016.

[44] O. Bazan and M. Jaseemuddin, "An opportunistic directional MAC protocol for multihop wireless networks with switched beam directional antennas," in *Proceedings of the IEEE International Conference on Communications, ICC 2008*, pp. 2775–2779, China, May 2008.

[45] M. J. Farooq, H. Elsawy, and M.-S. Alouini, "A Stochastic Geometry Model for Multi-Hop Highway Vehicular Communication," *IEEE Transactions on Wireless Communications*, vol. 15, no. 3, pp. 2276–2291, 2016.

[46] A. Corana, M. Marchesi, C. Martini, and S. Ridella, "Minimizing multimodal functions of continuous variables with the 'simulated annealing' algorithm," *ACM Transactions on Mathematical Software*, vol. 13, no. 3, pp. 262–280, 1987.

[47] W. K. Lai and G. G. Coghill, "Channel Assignment through Evolutionary Optimization," *IEEE Transactions on Vehicular Technology*, vol. 45, no. 1, pp. 91–96, 1996.

[48] J. Kennedy, "Particle swarm optimization," in *Encyclopedia of Machine Learning*, pp. 760–766, Springer US, Boston, MA, USA, 2011.

[49] P. S. Oliveto, J. He, and X. Yao, "Time complexity of evolutionary algorithms for combinatorial optimization: A decade of results," *International Journal of Automation and Computing*, vol. 4, no. 3, pp. 281–293, 2007.